

Nanofluids improve energy efficiency of membrane distillation

Harsharaj Parmar, Hamid Fattahijuybari, Yashwant Yogi,
Sina Nejati, Ryan Jacob, Prashant Menon,
David Warsinger¹

¹Department of Mechanical Engineering, Purdue University

December 31, 2020

1 Abstract

Thermal desalination of high salinity water resources is energy intensive and optimizing its energy efficiency can supplement the freshwater supply. Energy absorbing nanoparticles have improved the solar desalination efficiencies but using them in the feed as nanofluids can lead to substantial convective heat transfer in membrane distillation (MD). We modelled the dominant micro-mixing from Brownian motion in copper oxide nanofluids and the unusually high axial conduction from Van der Waals interaction in carbon nanotube nanofluids. Carbon nanotubes resulted in consistent, wide range of improvements; while copper oxide particles showcased diminishing returns after a concentration of 0.7%, where Brownian motion effects became negligible. Nanofluid characterizations illustrated uniform dispersions after atleast 75 minutes of sonication and using surfactants to stabilize the nanoparticles through micelle formations. However, the enhancements from liquid layering at higher nanofluid concentrations were impractical in MD, since the related high surfactant levels compromised the membrane hydrophobicity and promoted fouling. Dilute solutions of metallic nanofluids can be actively

integrated to enhance the performance of MD, whereas stronger nanofluid solutions should be limited to heat exchangers that supply thermal energy to MD systems.

2 Graphical Abstract

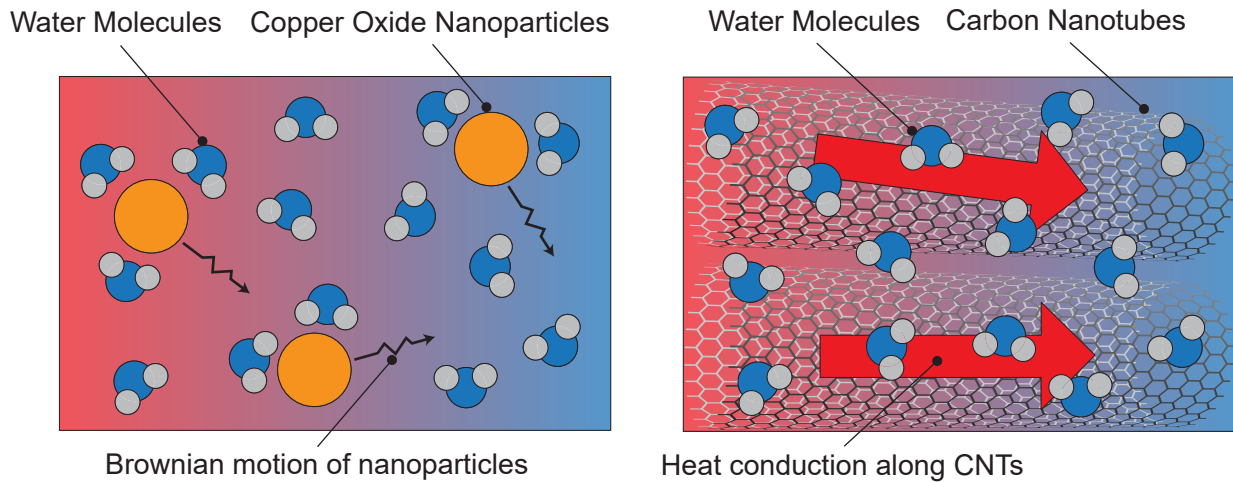


Figure 1: Schematic showing the mode of heat transfer enhancement using cooper oxide nanoparticles and carbon nanotubes in a distilled water basefluid. Brownian motion and the associated micro-mixing is the dominant mechanism for improved heat transfer in copper oxide nanofluid. Van der Waals interaction of carbon nanotubes results in a substantially high axial heat conduction across the fluid.

3 Introduction

3.1 The need for thermal desalination

Freshwater resources are being substantially overexploited around the world to meet rising water demand. The desalination of alternative sources like seawater, brackish water presents a possible solution, but the concentration to highly saline feeds tends to be energy intensive [1, 2]. Commercial pressure-driven desalination processes like reverse osmosis are impractical at high salt concentrations [3–5] and thus the general consensus is that improvements of thermal desalination technologies are needed for high salinity and high water recovery applications.

3.2 Membrane Distillation

One of the emerging thermal desalination processes - membrane distillation (MD) has particularly shown the ability to retain performance at high salinities [6]. From a broad perspective, MD systems reveal a close resemblance to counterflow heat exchangers with an added membrane between the two channels [7]. The hydrophobic membrane prevents the permeation of non volatile salts [8] to separate the hot feed stream (brine) and the cold distillate stream (pure water). Temperature difference between the two sides of the membrane results in a vapor pressure gradient that drives the desalination [9]. However, the inherent phase change in MD leads to proportionally high energy costs, which often constitute about two-thirds of the total operating expense [13]. Optimizing the heat and mass transfer in MD is therefore crucial because even minor improvements in efficiency can reflect as major industrial cost savings.

The temperature difference across MD membranes governs the pure water flux but also leads to significant heat conduction losses. In order to eliminate these losses, air gap membrane distillation (AGMD) [14, 15] introduces a thick air layer between the membrane and condensing surface. The additional MD configurations are classified by the properties of the gap between the membrane and condensing surface, like permeate gap membrane distillation (PGMD) [16,17] where the gap is flooded with water and conductive gap membrane distillation (CGMD) with high gap conductance [18,19]. In all these configurations, the vapor condenses within the gap and effective phase change regimes have demonstrated significant performance enhancements [20–22]. However, these modifications are often beneficial when flux stability is achieved from improved feed channel heat transfer using turbulence promoters [23] and corrugations [24] but such channel structures are optimized for specific flow conditions. As a result, methods that can preserve the feed heat transfer enhancements across varied operating conditions are desirable.

3.3 Heat transfer enhancements via nanofluids

Intrinsic fluid properties, notably thermal conductivity, directly affect the heat transfer and can be modified to attain performance improvements [25, 26]. To do so, high thermal

conductivity nanofluids have been used in heat exchangers (15%-41% enhancements at concentrations of 0.1%-2%) [27–30], and their application is extended to MD here. Nanofluids are formed by suspending highly conductive nanoparticles (with size scales below 100 nm) in low conductivity base solutions [31–33]. Nanoparticles affect the thermal transport properties of the base fluid, improving thermal conductivity by mainly two mechanisms [34]. First, the static dispersion of particles results in simple concentration-based linear enhancements [35, 36], which fail to explain the significant conductivity increments observed in extremely dilute nanofluids [37–42]. These low concentration improvements are attributed to the second enhancement mechanism; the random motion of nanoparticles in the solution, also known as Brownian motion [43]. Randomly moving particles with high surface energy carry packets of fluid around, resulting in a phenomena called micro-mixing [44, 45]. Such micro-scale interactions in the fluid lead to a lower local temperature gradient for a given heat flux which, macroscopically translates to higher thermal conductivity. Nanoparticle-based thermal collectors have enhanced the productivity of solar stills and flashing desalination systems [46–51]. Additionally, immobilized nanoparticles in solar MD membranes effectively concentrated the solar radiation near the membrane to achieve higher permeate flux [52, 53]. However, these studies used nanoparticles to absorb thermal energy instead of explicitly improving the convective heat transfer using nanofluids.

To examine the performance of nanofluids in MD, here we presented a comprehensive energy efficiency analysis of the leading MD configurations (AGMD, PGMD and CGMD) with carbon nanotubes (MWCNT) and copper oxide (CuO) nanoparticles in the feed channels. The effects of particle size, concentration and temperature on the thermal conductivity were modelled and benchmark efficiency metrics were calculated from these heat transfer enhancements. Characterization of nanofluids was done using SEM imaging and dynamic light scattering (DLS) to analyse the stable particle size distribution in the solution. From these results, we determined the agglomeration mechanisms in nanofluids emphasizing the role of surfactants in solution stability. Finally, the effects of nanofluids on membrane fouling and surface hydrophobicity were investigated by measuring the static contact angle of water and SEM characterization of the fouled membranes.

4 Materials and Methods

Methods overview: Nanofluids were created by adding purchased nanoparticles along with surfactants to a base deionized water solution and mixed with stirring and sonication to disperse the nanoparticles. Dynamic light scattering (DLS) was carried out to determine the agglomerate sizes in nanofluids after different sonication durations. Thereafter, SEM images of dried nanofluid solutions and fouling tested membranes were taken to visualize the particle dispersion. The contact angle of water on fouling tested membranes was measured to study their hydrophobicity after exposure to nanofluids. Finally, the thermal conductivity enhancements and property variations (density, specific heat and viscosity) of nanofluids were modelled to estimate the energy efficiency of MD systems using a comprehensive thermodynamic framework.

Materials and chemicals: Multi-walled carbon nanotubes (MWCNTs) with 9.5 nm average diameter, 1.5 μm average length, 250 m^2/g specific surface area and 90% purity were purchased from Nanocyl SA (Nanocyl SA, Sambreville, Belgium). Copper(II) oxide (CuO) nanoparticles with 10 nm average diameter and 99% purity, Polyvinylpyrrolidone (PVP, average MW 40,000) and Sodium dodecylbenzene sulfonate (SDBS, Purity > 99%) surfactants were obtained from Sigma-Aldrich (Sigma-Aldrich, St. Louis, MO). Unlaminated polytetrafluoroethylene (PTFE) membrane with pore size 0.2 μm , porosity 0.8, and thickness 50 μm was purchased from Sterlitech (Sterlitech, Kent, WA).

4.1 Experimental methods

Preparation of Nanofluids: Copper oxide nanoparticles (for CuO-Water nanofluid) or multi-walled carbon nanotubes (for MWCNT-Water nanofluid) were added to a solution of SDBS surfactant mixed with deionized water, as shown in Figure 2. Magnetic stirring was carried out to break down the macroscopic lumps of SDBS and nanoparticles in the solution. In order to get nanometer scale particles, the nanofluid was subsequently sonicated (Q700 Sonicator, Qsonica, Newtown, CT) at 45% vibration amplitude and 20 kHz frequency. The SDBS surfactant helped in stabilizing the nanoparticles agglomerating in the solution and the required sonication duration varied with the desired nanofluid concentration (6 different

samples were made as shown in Table 1).

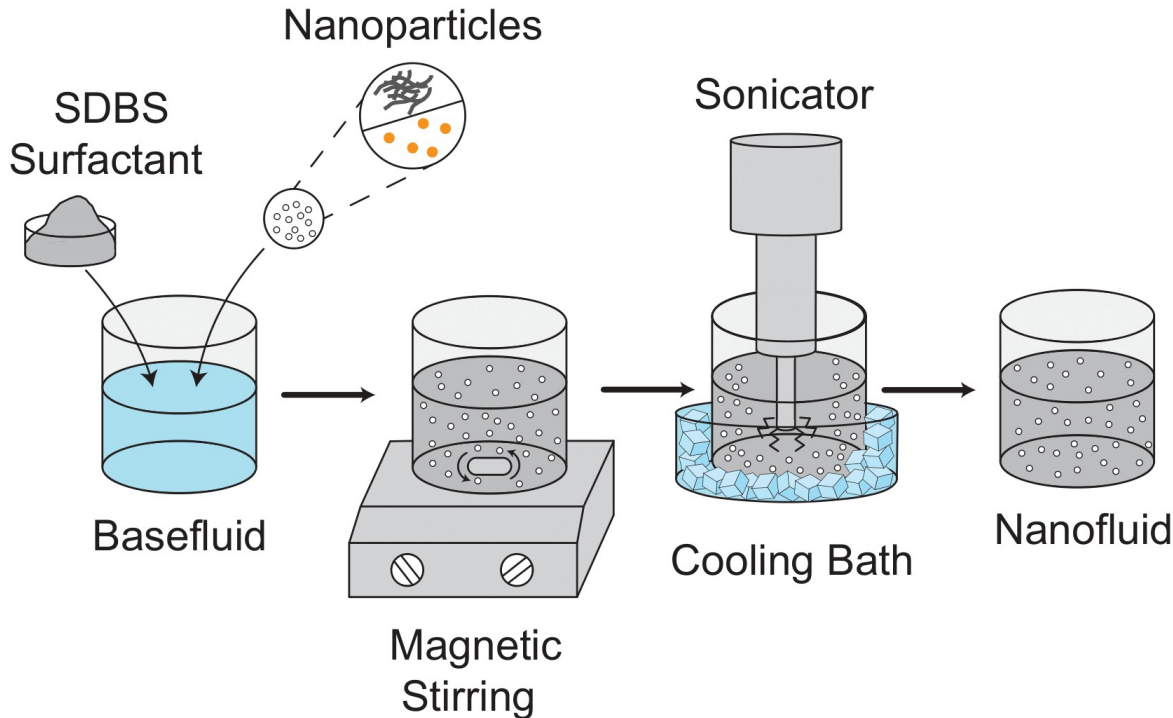


Figure 2: Nanofluid preparation using sodium dodecylbenzenesulfonate (SDBS) surfactant and sonication. Copper oxide nanoparticles are shown as orange spheres and multi-walled carbon nanotubes are represented by gray stands (top, middle).

Membrane Fouling Studies: Nanofluid solutions (copper oxide and carbon nanotubes) were circulated in a lab-scale MD module to investigate their effects on the fouling and hydrophobicity of a PTFE membrane. A 800 ml of 0.1% nanofluid solution was pumped through the feed channel for 2 hours, at a constant flow rate of 1 litre/min and a temperature of 50°C where fouling occurred. The module was flushed with deionized water before and after the test to remove surface adhered impurities and nanoparticles. Finally, the membrane was cleaned under a steady stream of deionized water for 5 minutes and naturally dried for characterization.

Nanofluid and Membrane Characterization: The agglomerate sizes in nanofluids were analyzed with sonication duration using dynamic light scattering (DLS) model Malvern Zetasizer Nano ZS. 0.001% CuO-Water and MWCNT-Water nanofluids were prepared with two different SDBS surfactant concentrations (0.05 and 0.005%) and samples were taken from

Table 1: Copper oxide (CuO) and carbon nanotube (MWCNT) nanofluids characterized for MD, with details on their concentration and sonication duration

Sample	Nanoparticle concentration	Surfactant concentration	Sonication duration	Usage
1	0.001% CuO	0.005% SDBS	3 hours	DLS studies
2	0.001% CuO	0.05% SDBS	3 hours	DLS studies
3	0.1% CuO	0.3% SDBS	1 hr 20 mins	Membrane fouling
4	0.001% MWCNT	0.005% SDBS	3 hours	DLS studies
5	0.001% MWCNT	0.05% SDBS	3 hours	DLS studies
6	0.1% MWCNT	0.5% SDBS	1 hr 20 mins	Membrane fouling

the solutions at specific time intervals during 3 hr sonication runs of the nanofluids. The morphological characterizations of nanofluids and membrane fouling were obtained using field emission scanning electron microscopy (FESEM model Hitachi S-4800). Nanofluid solutions were dried on a glass plate before SEM imaging. Energy dispersive x-ray spectroscopy (EDS) was used to identify copper oxide nanoparticles in the fouling tested membrane.

4.2 Numerical modelling

The complex heat and mass transfer physics in MD have been studied extensively through numerical models to understand the effects of system parameters on their flux [54, 55] and energy efficiency [56–58]. The modelling approach used here was based on the work from Summer et al. [59], and its details can be found in previous publications [5, 7, 14, 15, 19, 20].

The computational MD model was based on one-dimensional finite difference method, where properties varied along the length and were assumed to be constant along the width. Mass and energy conservation equations were solved for each discretized control volume using the built-in property evaluation functions of engineering equation solver (EES) [60]. Span-wise property variations were accounted for using thin temperature and concentration boundary layers. The nanofluids were treated as homogeneous entities with properties

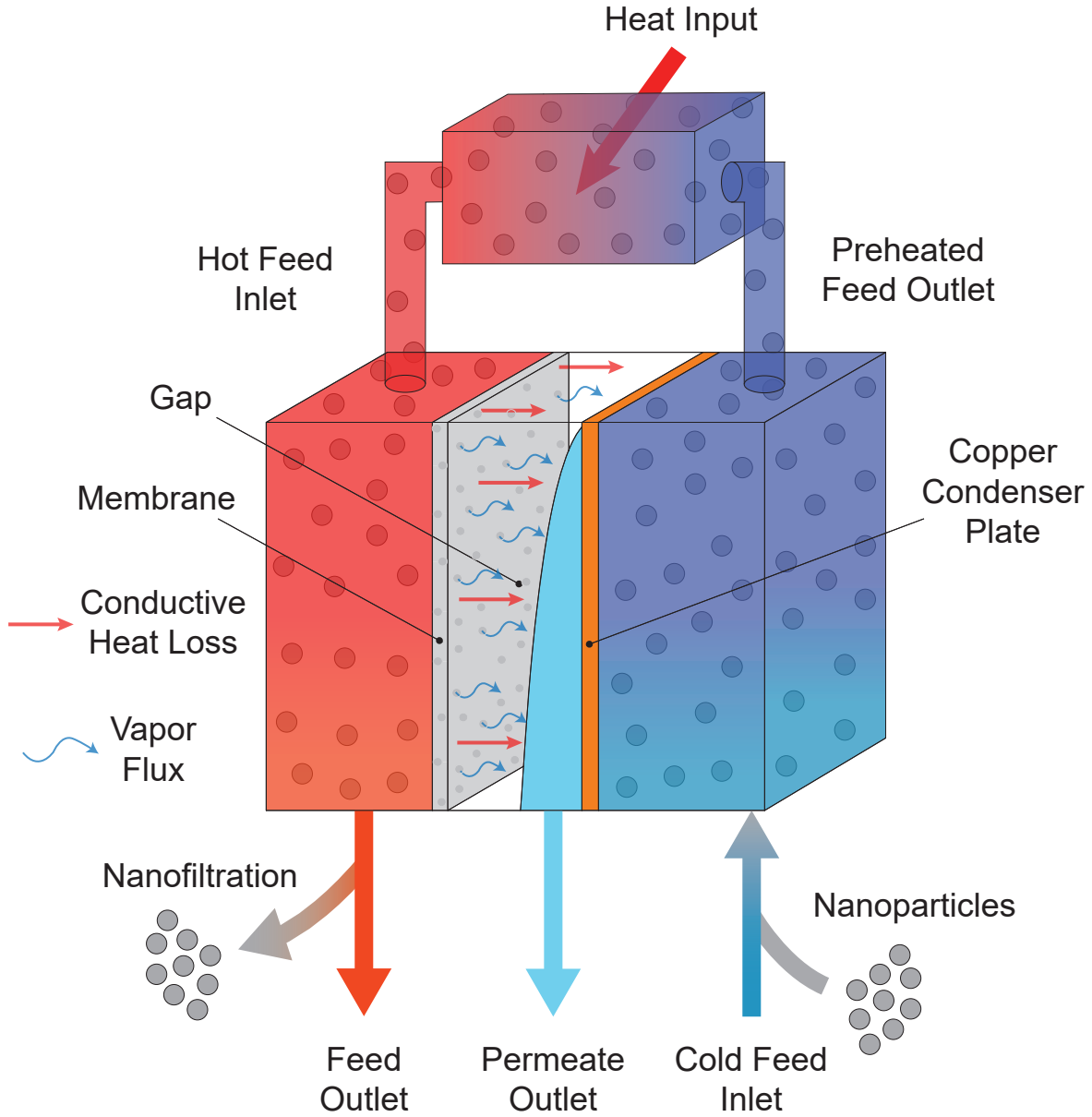


Figure 3: Membrane Distillation (MD) schematic with the addition of nanofluids. Three different configurations can be made by modifying the gap properties between the membrane and condenser plate. Air gap membrane distillation (AGMD), shown above, introduces a stagnant air medium in the gap region, permeate gap membrane distillation (PGMD) is obtained when the gap is flooded with water and finally conductive gap membrane distillation (CGMD) has conductive spacers stacked up in the gap.

modified according to relations from prior literature [61]. These relations included the effects

of temperature and material properties like particle size, volume fraction on the micro-scale particle dynamics.

4.2.1 Nanofluid thermal conductivity relations

Nanofluids exhibit unusual enhancements in thermal conductivity at very low nanoparticle concentrations and so numerous studies have been aimed at capturing this variation both analytically and experimentally [62–66].

In the present analysis, an analytical study from Koo et al. [67] on the variation of thermal conductivity was adopted for CuO-Water nanofluid. Numerous reviews have supported the validity of this relation with experimental data [61,66,68–72]. The conductivity enhancements with contributions from static particle dispersion and Brownian motion of particles were derived as shown below.

$$k_{\text{eff}} = k_{\text{static}} + k_{\text{brownian}}$$

The static enhancement expression used was identical to the one given by Maxwell [35],

$$\frac{k_{\text{static}}}{k_{bf}} = 1 + \frac{3\alpha_p \left(\frac{k_p}{k_{bf}} - 1 \right)}{\left(\frac{k_p}{k_{bf}} + 2 \right) - \alpha_p \left(\frac{k_p}{k_{bf}} - 1 \right)}$$

where α_p is the particle volume fraction, k_p is the thermal conductivity of nanoparticle and k_{bf} that of the base fluid. The brownian motion contribution to thermal conductivity was derived from time averaged kinetic theory [67, 73] and given as,

$$k_{\text{brownian}} = 5 * 10^4 \beta \alpha_p \rho_{bf} c_{bf} \sqrt{\frac{\kappa T}{\rho_p D}}$$

where ρ_{bf} is the density, c_{bf} is the specific heat of the base fluid, κ is the boltzmann constant, D the average diameter of particles and T the bulk temperature [67]. The term β is related to particle motion; it includes the effects of micro-mixing and is determined from experimental data. For CuO nanoparticles with concentration below 1% we have [67],

$$\beta = 0.0137 (100\alpha_p)^{-0.8229}$$

Carbon nanotubes have a fibrous structure and in order to accurately capture their interaction, a verified [74–76] experimental correlation from Esfe et al. [77] was used to model the

MWCNT-Water nanofluid. The correlation was valid for concentrations below 1% and for temperatures between 25 - 55°C which are prevalent in most MD systems.

$$\frac{k_{nf}}{k_{bf}} = \frac{(360.69 + T)}{(405.59 - 11080\alpha_p)}$$

4.2.2 Nanofluid properties: density, specific heat and viscosity

Density relations for nanofluids were derived assuming a simple static distribution of nanoparticles in the basefluid, and governed by a general fractional relation [78].

$$\rho_{nf} = \rho_p \alpha_p + \rho_{bf} (1 - \alpha_p)$$

where ρ_{nf} is the density of nanofluid and ρ_{bf} is the density of basefluid. The specific heat of nanofluids followed a similar concentration based relation given as [78],

$$c_{p,nf} = \left(\frac{\rho_p}{\rho_{nf}} \right) \alpha_p c_{p,p} + \left(\frac{\rho_{bf}}{\rho_{nf}} \right) (1 - \alpha_p) c_{p,bf}$$

where $c_{p,nf}$ represents the specific heat of nanofluid, $c_{p,bf}$ is the specific heat of basefluid and $c_{p,p}$ the specific heat of nanoparticles.

The dispersion of nanoparticles in the base fluid increases the viscosity of the solution, and as a result, nanofluid viscosity correlations have been studied extensively [72, 79] to quantify the associated increased pressure drops. Here a well-validated correlation proposed by Naik and Sundar [80] was used to model the viscosity changes with particle concentration and temperature for CuO-Water nanofluids.

$$\frac{\mu_{nf}}{\mu_{bf}} = 3.444 \left(\frac{T_{max}}{T_{min}} \right)^{0.514} \alpha_p^{0.1829}$$

The viscosity of MWCNT-Water nanofluids was modelled using a correlation from Esfe et al. [77] given as,

$$\frac{\mu_{nf}}{\mu_{bf}} = 38.158\alpha_p - 0.0017357T + 1.1296$$

where μ_{nf} represents the viscosity of nanofluid and μ_{bf} the viscosity of basefluid.

5 Results and Discussion

The performance of MD systems implementing nanofluids was quantified numerically along with investigating particle size, dispersion with sonication duration, surfactant concentration

and the effects of nanofluids on membrane fouling and hydrophobicity. First, the variation of thermal conductivity with particle concentration was studied at the average operating temperature of MD modules in section 5.1. The micro-mixing from Brownian motion significantly increased the heat transfer in copper oxide nanofluids and the Van der Waals interaction of carbon nanotubes led to substantial axial conduction across the basefluid, improving its thermal conductivity. Thereafter, the efficiency enhancements with varying nanoparticle concentration were compared for different MD configurations outlining the relative effects of improved channel heat transfer in section 5.2. The optimal performance of CGMD systems was studied with particle concentration to affirm new benchmark efficiency metrics for MD in section 5.3.

SEM images of dried nanofluid solutions were compared before and after sonication in section 5.4 to check for particle agglomeration. Particle interaction directly affected the nanoscale thermal transport, reducing the Brownian motion enabled mixing in copper oxide nanofluids and increasing the axial conduction across carbon nanotube nanofluids. Effects of SDBS surfactant and sonciation duration on the stable particle sizes in nanofluids were examined using the DLS technique in section 5.5. Finally, membrane fouling and hydrophobicity were tested in section 5.6 using SEM imaging and static contact angle measurements after circulating nanofluids in the MD module.

5.1 Modelled thermal conductivity enhancements from nanofluids

Thermal conductivity enhancements from carbon nanotubes and copper oxide nanoparticles were modelled for dilute nanofluids (below 1% concentration). Brownian motion and the related micro-mixing played a major role in increasing the thermal conductivity at very low nanofluid concentrations as seen in Figure 4a. When increasing the nanoparticle concentration, agglomeration was amplified, resulting in larger particles and reducing the significance of Brownian motion. Static enhancements dominated the thermal conductivity of nanofluids at higher concentrations, eventually tapering off the conductivity curve, as seen with copper oxide nanoparticles in Figure 4a. The static conductive transport was particularly prominent in nanotubes where axial interactions led to long chains carrying heat across the fluid (higher slope in 4a) [81]. Moreover, the increased particle density for nanotubes resulted

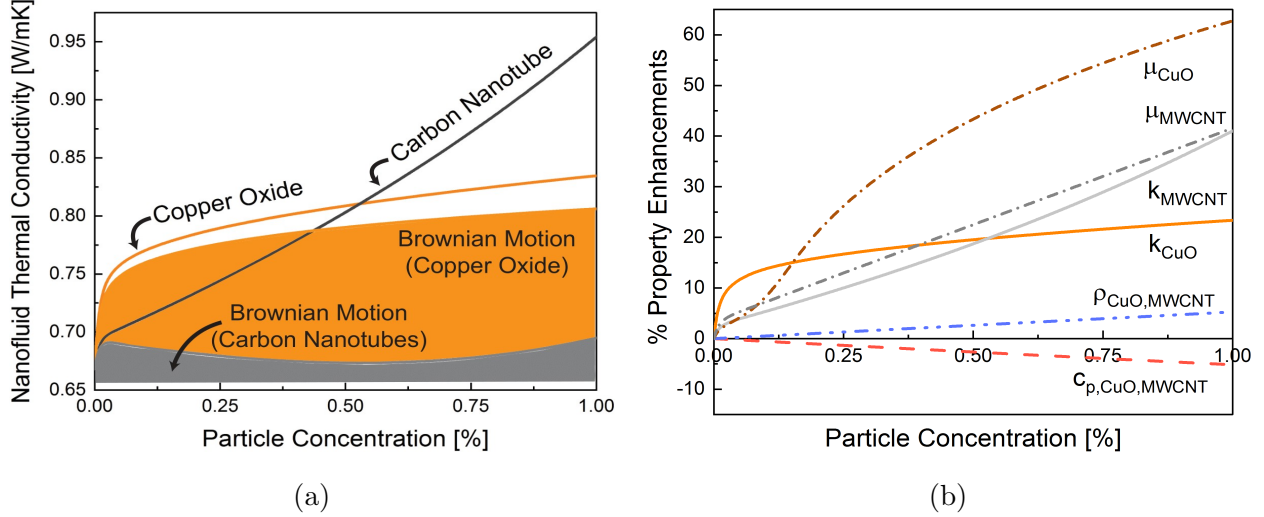


Figure 4: **Property variations in nanofluids:** (a) Variation of thermal conductivity for CuO-Water and Carbon Nanotube (MWCNT)-Water nanofluid by particle volume fraction, where contributions to thermal conductivity from Brownian motion are shown by shaded regions. (b) Property changes relative to seawater in the feed at various nanoparticle concentrations, including viscosity μ , density ρ , heat capacity c_p and conductivity k . Properties were evaluated at an average temperature of the MD system (55°C). Brownian motion and the interaction of particles significantly increases the nanofluid thermal conductivity compared to seawater (0.668 [W/mK]).

in significantly lower Brownian enhancements compared to copper oxide and showed an early transition to static thermal transport [82].

5.2 Relative energy efficiency of various MD configurations

The energy efficiency of thermal desalination systems is described by gained output ratio (GOR), which is defined as heat of vaporization of permeate divided by the heat input required for the MD system [83].

$$\text{GOR} = \frac{\dot{m}_{per} h_{fg}}{\dot{Q}_h}$$

where \dot{m}_{per} [kg/s] represents the permeate flux output from MD system, h_{fg} [kJ/kg] is the latent heat of vaporization and \dot{Q}_h [kW] is the thermal energy input required. Practical MD systems have GOR values ranging from 3-7 [19, 84, 85] with new configurations like

vacuum-assisted air gap membrane distillation (V-AGMD) [86] peaking at 13.5.

Percentage efficiency enhancements from the nanofluids were calculated compared to using seawater in the feed channel, and plotted at varying particle concentration as shown in Fig. 5 (modelling conditions given in Appendix A.1). The dominant heat transfer resistance of the gap region in AGMD and PGMD, limited the optimum energy benefits from using nanofluids in the feed channels. On the other hand, the CGMD configuration with high gap conductance showed remarkable increments in energy efficiency and proved to be more sensitive to the improved feed heat transfer.

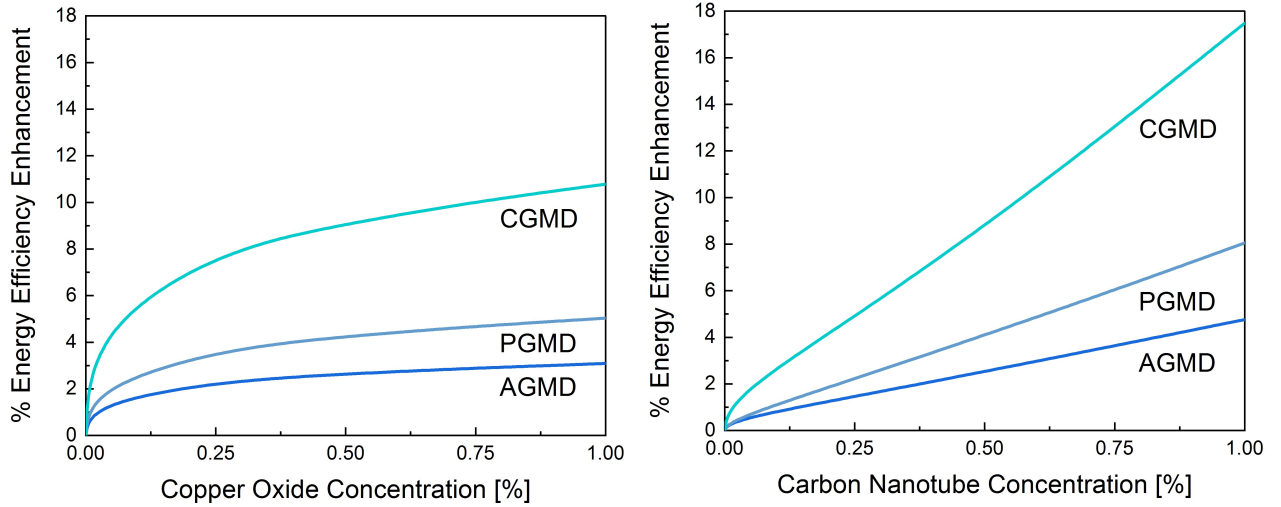


Figure 5: Nanofluid improvements by MD configuration: Relative enhancement of energy efficiency (GOR) with nanoparticle volume fraction for AGMD, PGMD and CGMD configurations. Operating conditions were ensured to be uniform across all the configurations, and for the CGMD model, the gap thermal conductivity was set to $k_{gap} = 10[W/mK]$. Enhancements follow the thermal conductivity plot (Figure 4a) for both copper oxide and carbon nanotubes. AGMD and PGMD configurations showed lower enhancements due to a dominant gap heat transfer resistance.

5.3 Benchmark efficiency metrics for conductive gap MD systems

Modelling the energy efficiency enhancements in section 5.2, we observed that CGMD systems show substantial improvements using nanofluids in the feed channel. The maximum

attainable energy efficiency of CGMD systems incorporating nanofluids was then evaluated at different nanoparticle concentrations (Figure 6).

Here, we see that increasing the gap thermal conductivity in CGMD promoted higher efficiencies, but quickly had diminishing returns above $k \approx 10$ W/mK value, as shown in Figure 6. We observed that energy efficiency changes very little above a threshold gap thermal conductivity, where the thermal resistance of the gap becomes negligible [19]. This plot provided an estimation of the benchmark performance of MD resulting from improved feed channel heat transfer using nanofluids and a highly conductive gap in CGMD.

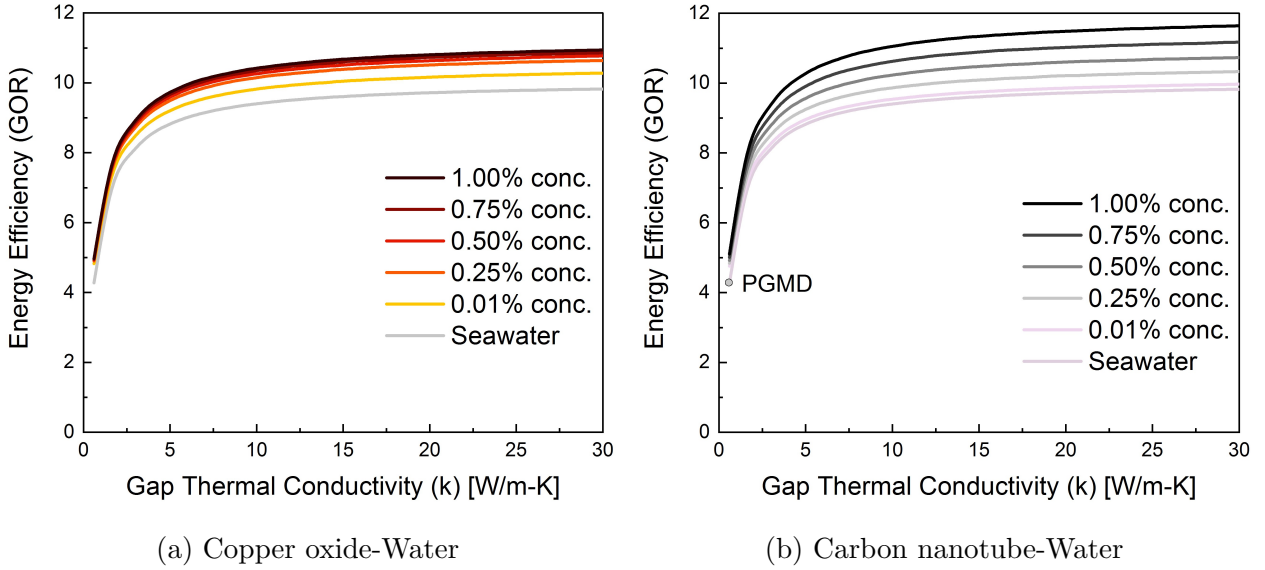


Figure 6: **Energy efficiency (GOR) vs gap thermal conductivity** for a CGMD configuration using nanofluids in the feed channels. Nanoparticle concentration was varied for copper oxide and carbon nanotubes along with changes to the gap thermal conductivity. A point for water flooded gap enhancement (PGMD) is also shown for comparison. The optimal performance does not change much for copper oxide nanoparticles after a concentration of roughly 0.7%, whereas carbon nanotubes show more continuous improvements. The difference is likely due to separate thermal mechanisms being dominant, as copper oxide nanofluids are highly dependant on Brownian motion, which is reduced by agglomeration at higher nanofluid concentrations.

5.4 Particle dispersion after sonication of nanofluids

The clustering of nanoparticles significantly affects the thermal conductivity enhancements [87] and as a result, the stabilization of nanofluids using sonication and surfactants is critical. The increase in particle sizes hinders the Brownian motion at low concentrations [70, 88, 89] but results in effective liquid layering at higher concentrations [90]. This indicates that clustering reaps benefits to a certain extent, however, can also lead to sedimentation at larger characteristic sizes [91].

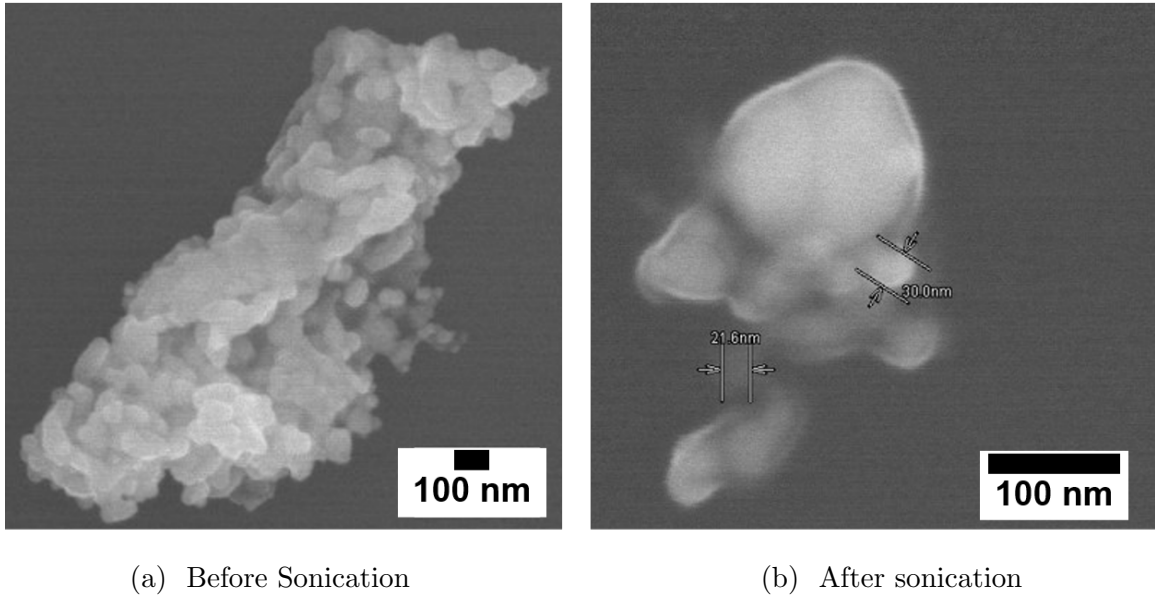
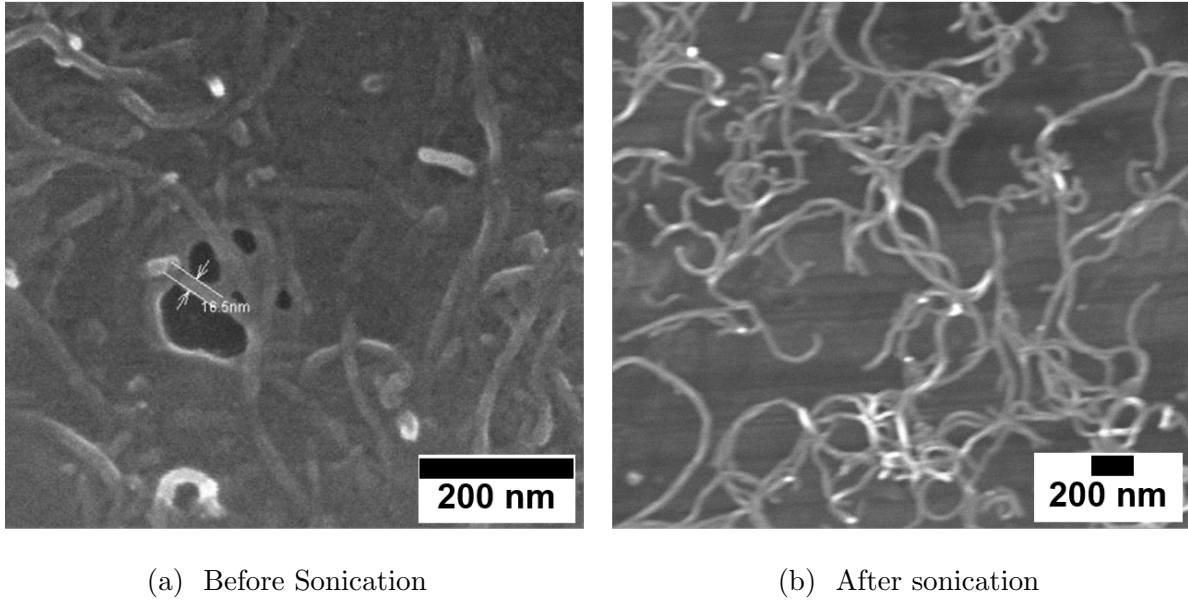


Figure 7: Sonication of copper oxide nanofluid: Agglomerate size comparison for a dried sample of 0.001% CuO-Water nanofluid with 0.005% SDBS, before and after 2 hours of sonication. Sonication breaks down the nanoparticles, which then interact again in the solution and are stabilized using surfactants. Copper oxide clusters of the order of $1\ \mu\text{m}$ were broken down to characteristic size scales smaller than 200 nm, which effectively contributed to thermal conductivity enhancements from their Brownian motion.

We investigated the effects of sonication, surfactant addition on the stability of nanofluids and used SEM imaging to visualize the particle dispersion. The particles in a magnetically stirred nanofluid solution were compared with those in another solution sonicated for 2 hours at the same concentration. Sonication of the nanofluid reduced the micro-scale structures in the solution to nanometer sized particles for copper oxide (Figure 7) and distinct nanometer



(a) Before Sonication

(b) After sonication

Figure 8: Sonication of MWCNT nanofluid: Effects of sonication on the clustering of nanotubes in a 0.001% MWCNT-Water nanofluid with 0.005% SDBS solution sample dried on a glass plate. Carbon nanotubes showed massive agglomeration after magnetic stirring and were widely dispersed after 2 hours of sonication. The length of nanotube agglomerates stayed above 500 nm even after sonication due to their strong axial interaction forces. These long, surfactant stabilized nanotube strands reduce the Brownian motion but are very effective in static conduction across the fluid.

scale strands for carbon nanotubes (Figure 8). Moreover, the characteristic size scales observed in Figure 7 and 8 after sonication were larger than the nominal copper oxide particles and carbon nanotubes respectively. This indicated that particle interaction was prominent during sonication and the resulting agglomerates were stabilized through micelle structures formed by the surrounding surfactant molecules in the solution.

5.5 Particle size analysis with dynamic light scattering

In order to determine the optimal surfactant concentration and sonication duration for stable solutions, we performed dynamic light scattering (DLS) studies on the nanofluids. The average particle sizes of copper oxide and carbon nanotubes decreased significantly after 20 minutes of sonication as shown in Figure 9 and then attained stability, where the interaction

of nanoparticles balanced their break-up from sonication. We observed that the amount of SDBS in the solution affected the particle sizes and above a concentration of 0.01%, SDBS showed decreased effectiveness (for a 0.001% nanofluid concentration). From the results obtained in Figure 9, we concluded that stable solutions can be made by using roughly 5 times more SDBS concentration than the required nanofluid concentration and performing atleast 75 minutes of sonication. Moreover, prolonged exposures to sonication (3 hour duration in Figure 9) resulted in the formation of bubbles in the nanofluids which inhibited the cluster breakage and led to a substantial increase in the average particle size [92]. Several studies on metal oxide [92–94] (alumina, zirconia and titanium dioxide) and carbon nanotube [95] nanofluids have reported this unusual observation with some cases leading to structural defects in the nanoparticles.

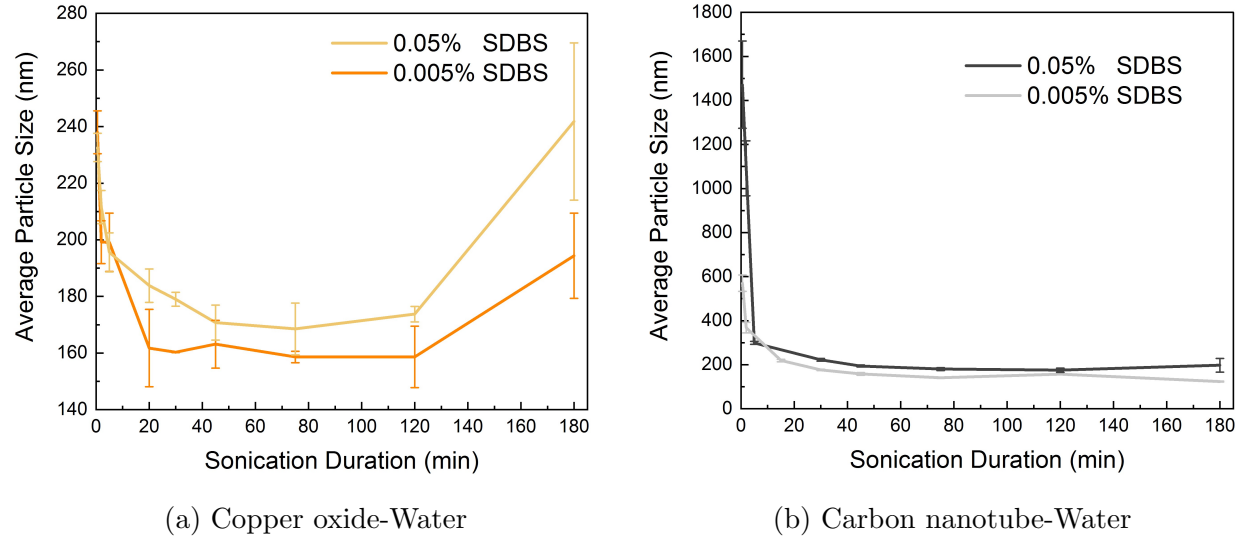


Figure 9: Nanofluid particle size vs sonication, via dynamic light scattering: Variation of average particle size of copper oxide and carbon nanotubes with sonication duration for two different concentrations of SDBS surfactant (0.05% and 0.005%). The SDBS surfactant acts to stabilize the nanoparticles in the solution and prevent agglomeration, however, above a concentration of 0.01% it showed reduced effectiveness (yellow, 0.05%). Particle sizes increased abruptly after longer sonication durations for CuO-Water and MWCNT-Water (0.05%) nanofluid due to the development of stable air bubbles in the solution which inhibited the nanoparticle cluster breakage.

5.6 Effects of nanofluids on membrane fouling and hydrophobicity

While the surfactants help in dispersion of the nanofluids, they pose a risk to MD because they reduce the surface tension of the feed water, which can compromise the hydrophobicity of PTFE membranes [96]. As the membrane loses its hydrophobicity, mineral salts from the feed can permeate through the membrane affecting distillate quality and flux production [97, 98]. Nanofluids in the feed channel can aggravate this issue by fouling the wetted membrane, where the nanoparticles adhere to the membrane surface reducing its permeability. We investigated the effects of nanofluids with SDBS surfactant on the membrane fouling, surface hydrophobicity using SEM imaging and static contact angle measurements of water.

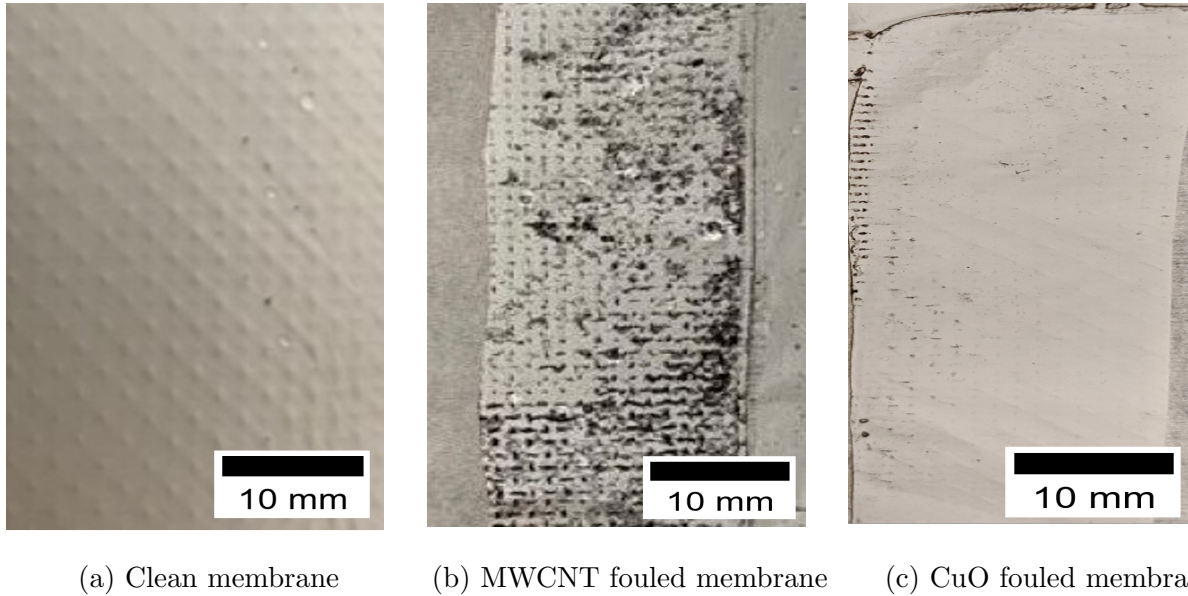


Figure 10: **Macroscopic images of PTFE membrane after fouling tests** with MWCNT and copper oxide nanofluids. Part (a) shows a clean PTFE membrane and (b), (c) show the fouled counterparts, flushed with water for 5 minutes to remove the loosely adhered particles. Carbon nanotubes show substantial membrane fouling at the macroscale due to their higher particle density in comparison to copper oxide nanoparticles.

Macroscopic images of the PTFE membrane (Figure 10) after fouling tests with nanofluids, showed significant carbon nanotube deposits in comparison to copper oxide nanoparticles. MWCNT nanofluids resulted in extensive fouling of the membrane with nanotubes interacting at the microscale with PTFE fibres as seen in Figure 12. Copper oxide nanoparticles on

the other hand, showed very little fouling with some microscale agglomerate deposition on the membrane (Figure 11). We observed that the SDBS surfactant used for preparing the nanofluids affects the membrane hydrophobicity; eventually allowing nanoparticles to foul parts of the membrane. In order to quantify the decreasing membrane hydrophobicity, we measured the static contact angle of water on the fouling tested membrane samples and compared the results with that of a clean PTFE membrane.

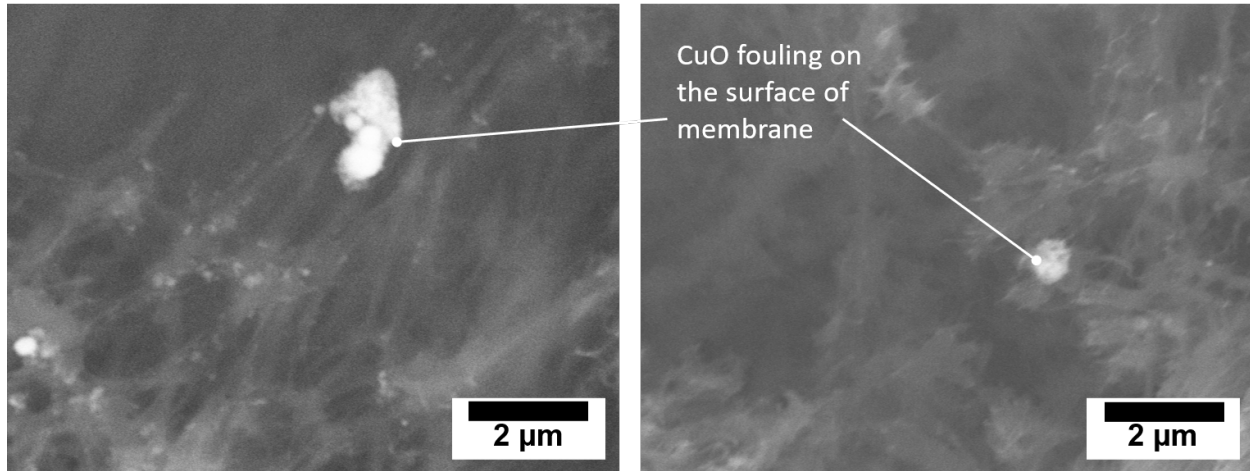


Figure 11: Membrane fouling from copper oxide nanoparticles: SEM micrographs of the membrane after fouling tests with 0.1% CuO-Water nanofluid. Negligible membrane fouling is observed using copper oxide with very few micrometer scale agglomerates interacting with the membrane fibres. Energy dispersive x-ray spectroscopy (EDS) was used to identify the copper oxide nanoparticles in the membrane.

The static contact angle of water on the membrane decreased after fouling studies with nanofluids indicating a marginal loss in membrane hydrophobicity (Figure 13). The contact angle measurements after using nanofluids were similar for both copper oxide and carbon nanotubes with the latter showing slightly higher variations. This was expected since the concentration of SDBS was the same in both the samples and thus would equally affect the hydrophobicity. The large variations in measurement for carbon nanotubes were the result of an uneven membrane surface caused by extensive fouling. We concluded that the SDBS surfactant marginally decreases the membrane hydrophobicity resulting in fouling from nanoparticles. The extent of membrane fouling can be reduced by using nanoparticles

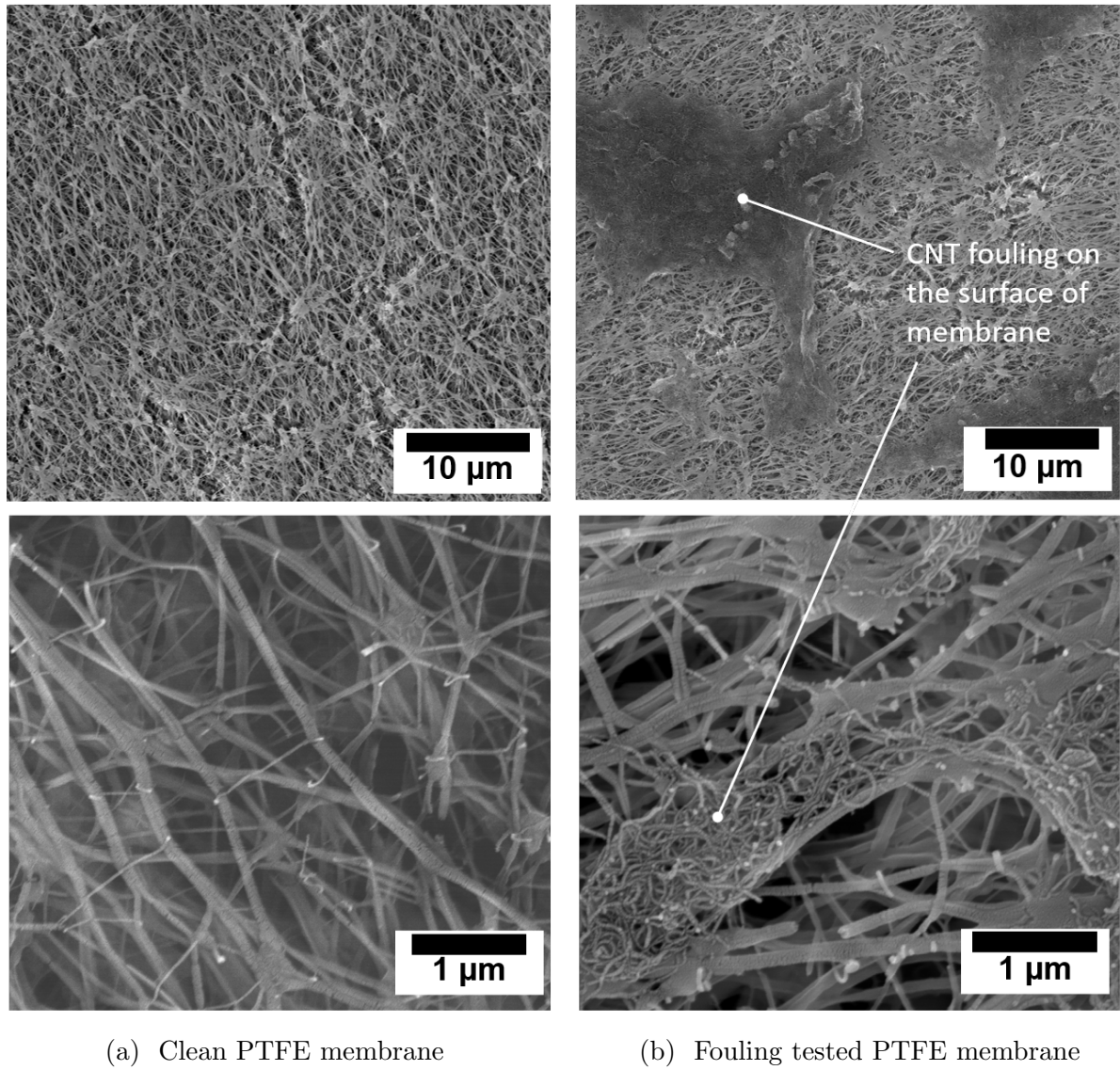


Figure 12: Membrane fouling from carbon nanotubes: SEM images showing the fouling of a PTFE membrane using 0.1% MWCNT-Water nanofluid. Dark black spots on the right hand side images show significant clustering of carbon nanotubes on the membrane surface and interactions with the membrane fibres at the microscale. SDBS surfactant reduces the surface tension of the feed, decreasing the membrane hydrophobicity and allowing nanoparticles to interact with the membrane. Nanotubes have a very high number density (number of particles per unit volume) and as a result, showed extensive membrane fouling.

that have lower number densities (number of particles per unit volume).

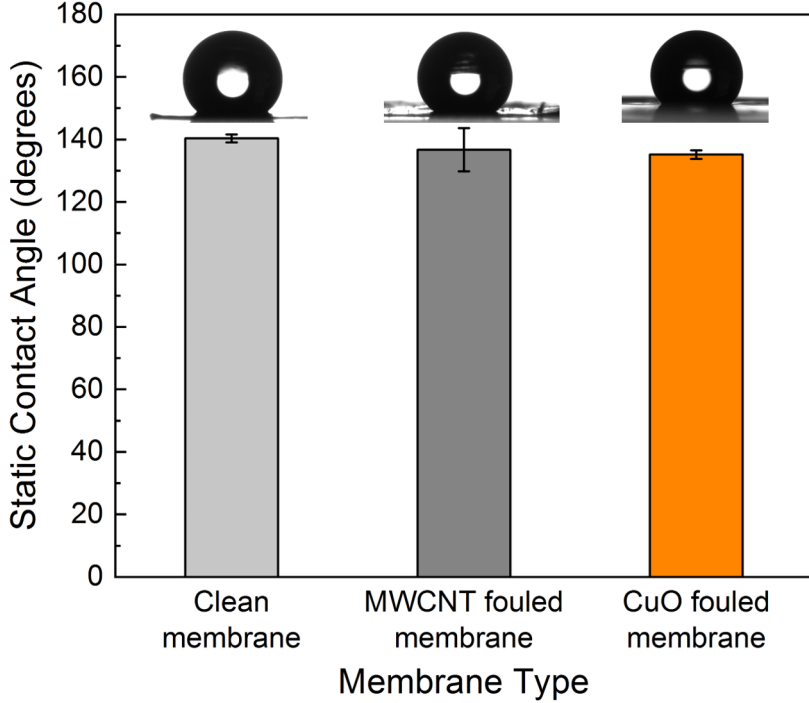


Figure 13: Hydrophobicity comparison of the fouled membranes: Static contact angle of water on a clean PTFE membrane and two nanofluid fouling tested PTFE membrane samples. The reduction in membrane hydrophobicity is nearly equal after using CuO-Water and MWCNT-Water nanofluids in the feed channel, since they have the same SDBS surfactant concentration. The carbon nanotube fouled membrane sample shows a relatively higher variation in measurements due to the uneven membrane surface caused by significant nanotube deposition.

6 Conclusion

Metallic nanoparticles of characteristic size scales below an order of 100 nm can result in effective micro-mixing of the feed from their Brownian motion at low concentrations. The Van der Waal interaction of fibrous nanotubes can achieve even higher static conduction enhancements across the nanofluid. The improvements in heat transfer from these mechanisms can promote significantly higher efficiencies in membrane distillation across diverse operating conditions and system scales. However, as we demonstrated from nanofluid characterization, stable dispersions demand optimized sonication durations and surfactant concentrations. Moreover, surfactants reduced the membrane hydrophobicity and served as promoters for

membrane fouling affecting the performance of MD. Dilute solutions of metallic nanofluids showed minimal membrane fouling and can be used in the channels for significant heat transfer improvements. The fouling concerns of carbon nanotubes promote their usage in heat exchangers for thermal input to MD systems, instead of directly suspending them in the channels. The success of these enhancement mechanisms suggests that other magnetic nanoparticles and hybrid nonofluids can be used in MD owing to their controllability and ease of separation. Special membrane modifications that help in retaining their hydrophobicity at higher nanofluid concentrations can further push the performance frontiers in MD.

7 Acknowledgements

The authors would like to acknowledge Porous Materials Inc. (PMI). We would like to thank Mr. Rishav Roy, Purdue University for helping with the contact angle measurements and Ms. Yuhang Fang, Purdue University for assisting in SEM characterization. The authors are grateful to Ms. Katherine Young, Purdue University for helping with the artwork and Mr. Timothy Simon, Purdue University for providing purchasing information on nanofluids. We also thank the group members who have had direct or indirect contributions in facilitating this work.

Nomenclature

Acronyms

AGMD air gap membrane distillation

CGMD conductive gap membrane distillation

CuO copper oxide

DLS dynamic light scattering

EDS energy dispersive x-ray spectroscopy

GOR gained output ratio

MD membrane distillation

MWCNT multi-walled carbon nanotubes

PGMD permeate gap membrane distillation

PTFE polytetraflouoroethylene

SDBS sodium dodecylbenzene sulfonate

SEM scanning electron microscopy

Greek symbols

α_p particle volume fraction

β particle motion modification

κ Boltzmann constant

μ viscosity, kg/m.s

ρ density, kg/m³

Roman symbols

- \dot{m} mass flow rate, kg/s
 \dot{Q} heat transfer rate, W
 c_p specific heat capacity, J/kg.K
 D average particle diameter, m
 h_{fg} enthalpy of vaporization, J/kg
 k thermal conductivity, W/m.K
 T temperature, K

Subscripts, superscripts

- bf basefluid
 brownian Brownian motion enhancements
 eff effective property of nanofluid
 gap gap between membrane and condenser plate
 max maximum
 min minimum
 nf nanofluid
 per permeate
 p particle
 static static enhancements

Appendix A

A.1 Model system parameters

Table 2: System parameters used in the numerical model

Parameter	Symbol	Value	Units
Membrane permeability coefficient	B_o	$2 * 10^{-10}$	s
Membrane thickness	δ_m	200	μm
Membrane porosity	ϕ	0.8	-
Membrane thermal conductivity	k_m	0.2	W/m K
Membrane width per unit flow rate	$w/\dot{m}_{f,in}$	12	m/(kg/s)
Module length	L	6	m
Top temperature	$T_{f,in}$	85	$^{\circ}\text{C}$
Seawater inlet temperature	$T_{sw,in}$	25	$^{\circ}\text{C}$
Channel height	d_{ch}	1	mm
Feed inlet salinity	Sal_{in}	35	g/kg
Gap thickness	d_{gap}	1	mm
Gap conductivity (CGMD)	k_{gap}	10	W/m K
Gap conductivity (PGMD)	k_{gap}	0.668	W/m K
Gap spacer conductivity (AGMD)	$k_{gap,spacer}$	0.2	W/m K
Specific heat capacity (copper oxide)	$c_{p,CuO}$	531	J/kg K
Density of copper oxide	ρ_{CuO}	6310	kg/m ³
Thermal conductivity of copper oxide	$k_{p,CuO}$	76.5	W/m K
Average particle diameter (CuO)	$D_{p,CuO}$	29	nm
Diffusivity of salt in water	$D_{s,w}$	$1.76 * 10^{-9}$	m ² /s

References

- [1] Goh, P.S., Matsuura, T., Ismail, A.F. and Hilal, N. *Recent trends in membranes and membrane processes for desalination.* Desalination 2016, 391, pp.43-60.
- [2] Al-Obaidani S., Curcio E., Macedonio F., Di Profio G., Ai- Hinai H., Drioli E. *Potential of membrane distillation in seawater desalination: Thermal efficiency, sensitivity study and cost estimation.* J. Membr. Sci. 2008, 323 (1), 85-98.
- [3] Li J. F., Guan Y. S., Cheng F. Q., Liu Y. *Treatment of high salinity brines by direct contact membrane distillation: Effect of membrane characteristics and salinity.* Chemosphere 2015, 140, 143-149.
- [4] Leitch, M. E., Li, C. K., Ikkala, O., Mauter, M. S., Lowry, G. V. *Bacterial Nanocellulose Aerogel Membranes: Novel High-Porosity Materials for Membrane Distillation.* Environ. Sci. Technol. Lett. 2016, 3 (3), 85-91.
- [5] Swaminathan J, Chung HW, Warsinger DM, Lienhard V JH. *Energy efficiency of membrane distillation up to high salinity: Evaluating critical system size and optimal membrane thickness.* Applied Energy 2018, 211:715-734.
- [6] Lin S., Yip N.Y. and Elimelech M. *Direct contact membrane distillation with heat recovery: Thermodynamic insights from module scale modeling.* Journal of membrane science 2014, 453, pp.498-515.
- [7] Swaminathan J, Chung HW, Warsinger DM, Lienhard V JH. *Membrane distillation model based on heat exchanger theory and configuration comparison.* Applied Energy 2016, 184:491-505.
- [8] Lawson, K. W., Lloyd, D. R. *Membrane distillation.* J. Membr. Sci. 1997, 124 (1), 1-25.
- [9] Alkhudhiri A., Darwish N. and Hilal N. *Membrane distillation: A comprehensive review.* Desalination 2012, 287, pp.2-18.

- [10] Ghaffour N, Lattemann S, Missimer T, Ng KC, Sinha S, Amy G. *Renewable energy-driven innovative energy-efficient desalination technologies*. Applied Energy 2014, 136:1155-65.
- [11] Sarbatly R, Chiam C-K. *Evaluation of geothermal energy in desalination by vacuum membrane distillation*. Applied Energy 2013, 112:737-46.
- [12] Suarez F, Ruskowitz JA, Tyler SW, Childress AE. *Renewable water: direct contact membrane distillation coupled with solar ponds*. Applied Energy 2015, 158:532-9.
- [13] Khayet, M. *Solar desalination by membrane distillation: Dispersion in energy consumption analysis and water production costs (a review)*. Desalination 2013, 308, pp.89-101.
- [14] Warsinger DEM, Swaminathan J, Lienhard V JH. *Effect of module inclination angle on air gap membrane distillation*. In: Proceedings of the 15th international heat transfer conference, IHTC-15, paper no. IHTC15-9351, Kyoto, Japan, August 2014.
- [15] Warsinger DM, Swaminathan J, Maswadeh L, Lienhard V JH. *Superhydrophobic condenser surfaces for air gap membrane distillation*. J Membr. Sci. 2015, 492:578-87.
- [16] Winter D, Koschikowski J, Wieghaus M. *Desalination using membrane distillation: experimental studies on full scale spiral wound modules..* J Membr. Sci. 2011, 375(1-2):104-12.
- [17] Cipollina A, Di Sparti M, Tamburini A, Micale G. *Development of a membrane distillation module for solar energy seawater desalination*. Chem Eng. Res. Des. 2012, 90(12):2101-21.
- [18] Ma Z, Davis TD, Irish JR, Winch GD. *Membrane distillation system and method*. US patent app., 12/694,757 [January 27 2010].
- [19] Swaminathan J, Chung HW, Warsinger D, Al-Marzooqi F, Arafat HA, Lienhard V JH. *Energy efficiency of permeate gap and novel conductive gap membrane distillation*. J Membr. Sci. 2016, 502:171-8.

- [20] Warsinger DM, Swaminathan J, Morales LL, Lienhard V JH. *Comprehensive condensation flow regimes in air gap membrane distillation: Visualization and energy efficiency*. J Membr. Sci. 2018, 555(1-2):517-528.
- [21] Yogi Y, Parmar HB, Fattahijuybari H, Sett S, Li L, Roy R, Weibel JA, Miljkovic N, Warsinger DM. *Slippery liquid infused porous condenser surfaces (SLIPS) for high efficiency air gap membrane distillation*. Planned submission in Joule (2021).
- [22] Fattahijuybari H, Parmar HB, Warsinger DM. *Porous condensers for improved efficiency in membrane distillation*. Planned submission in Applied Energy (2021).
- [23] Yang x, Yu H, Wang R, Fane AG. *Analysis of the effect of turbulence promoters in hollow fiber membrane distillation modules by computational fluid dynamic(CFD)simulations*. J Membr. Sci. 2012, 415-416:758-69.
- [24] Kharraz JA, Bilad MR, Arafat HA. *Flux stabilization in membrane distillation desalination of seawater and brine using corrugated PVDF membranes*. J Membr. Sci. 2015, 495:404-414.
- [25] Xuan Y, Li Q. *Heat transfer enhancement of nanofluids*. International Journal of Heat and Fluid Flow 2000, 21:58-64.
- [26] Wen D, Ding Y. *Experimental investigation into convective heat transfer of nanofluids at the entrance region under laminar flow conditions*. International Journal of Heat and Mass Transfer 2004, 47:5181-5188.
- [27] Ghozatloo A, Rashidi A, Shariaty-Niassar M. *Convective heat transfer enhancement of graphene nanofluids in shell and tube heat exchanger*. Experimental Thermal and Fluid Science 2014, 53:136-141.
- [28] Trisaksri V, Wongwises S. *Critical review of heat transfer characteristics of nanofluids*. Renewable and Sustainable Energy Reviews 2007, 11:512-523.
- [29] Eastman, J. A., Choi, S. U. S., Li, S., Soyez, G., Thompson, L. J., and DiMelfi, R. J. *Novel Thermal Properties of Nanostructured Materials*. Journal of Metastable Nanocrystalline Materials 1998, 2:629-637.

- [30] Wen, D., and Ding, Y. *Experimental Investigation into Convective Heat Transfer of Nanofluids at the Entrance Region under Laminar Flow Conditions*. International Journal of Heat and Mass Transfer 2004, 47:5181-88.
- [31] Vajjha RS, Das DK. *A review and analysis on influence of temperature and concentration of nanofluids on thermophysical properties, heat transfer and pumping power*. International Journal of Heat and Mass Transfer 2012, 55:4063-4078.
- [32] Hussein AM, Sharma KV, Bakar RA, Kadirgama K. *A review of forced convection heat transfer enhancement and hydrodynamic characteristics of a nanofluid*. Ren. and Sus. Energy Rev. 2014, 29:734-743.
- [33] Chandrasekar M, Suresh S, Senthilkumar T. *Mechanisms proposed through experimental investigations on thermophysical properties and forced convective heat transfer characteristics of various nanofluids – A review*. Ren. and Sus. Energy Rev. 2012, 16:3917-38.
- [34] Webb RL. *Principles of Enhanced Heat Transfer*. John Wiley & Sons, New York, 1993.
- [35] Maxwell J. *A Treatise on Electricity and Magnetism. 2nd edn*. Oxford University Press, Cambridge, UK, 1904.
- [36] Hamilton R.L. and Crosser O.K. *Thermal conductivity of heterogeneous two-component systems*. Industrial & Engineering chemistry fundamentals 1962, 1(3), pp.187-191.
- [37] Xuan Y, Li Q. *Heat transfer enhancement of nanofluids*. International Journal of Heat and Fluid Flow 2002, 21:58-64.
- [38] Yang Y, Zhang ZG, Grulke EA, Anderson WB, Wu G. *Heat transfer properties of nanoparticle-in-fluid dispersions (nanofluids) in laminar flow*. International Journal of Heat and Mass Transfer 2005, 48:1107-16.
- [39] Rea U, McKrell T, Hu LW, Buongiorno J. *Laminar convective heat transfer and viscous pressure loss of alumina–water and zirconia–water nanofluids*. International Journal of Heat and Mass Transfer 2009, 52:2042-8.

- [40] Hwang KS, Jang SP, Choi S. *Flow and convective heat transfer characteristics of water-based Al₂O₃ nanofluids in fully developed laminar flow regime*. International Journal of Heat and Mass Transfer 2009;52:193-9.
- [41] Pak BC, Cho YI. *Hydrodynamic and heat transfer study of dispersed fluids with submicron metallic oxide particles*. Experimental Heat Transfer: A Journal of Thermal Energy Generation, Transport, Storage, and Conversion 1998;11:151-70.
- [42] Sajadi AR, Kazemi MH. *Investigation of turbulent convective heat transfer and pressure drop of TiO₂-water nanofluid in circular tube*. International Communications in Heat and Mass Transfer 2011; 38:1474-8.
- [43] Kebinski P., Phillipot S.R., Choi S.U.S. and Eastman J.A. *Mechanisms of heat flow in suspensions of nano-sized particles (nanofluids)*. International journal of heat and mass transfer 2002; 45(4), pp.855-863.
- [44] Xuan Y., Li Q. and Hu W. *Aggregation structure and thermal conductivity of nanofluids*. AIChE Journal 2003; 49(4), pp.1038-1043.
- [45] Lee D. *Thermophysical properties of interfacial layer in nanofluids*. Langmuir 2007; 23(11), pp.6011-6018.
- [46] Hussein AK. *Applications of nanotechnology to improve the performance of solar collectors – Recent advances and overview*. Renewable and Sustainable Energy Reviews 2016; 62:767-792.
- [47] Arunkumar T, Raj K, Denkenberger D, Velraj R. *Heat carrier nanofluids in solar still – a review*. Desalination and water treatment 2018; 130:1-16.
- [48] Goh PS, Ismail AF, Matsuura T. *Perspective and Roadmap of Energy-Efficient Desalination Integrated with Nanomaterials*. Separation & Purification Reviews 2018; 47(2):124-141.
- [49] Sharshir SW, Guilong P, Lirong W, Nuo Y, Essa FA, Elsheikh AH, Mohamed SIT, Kabeel AE. *Enhancing the solar still performance using nanofluids and glass cover cooling: Experimental study*. Applied Thermal Engineering 2017; 113:684-693.

- [50] Chen W, Zou C, Li X, Li L. *Experimental investigation of SiC nanofluids for solar distillation system: stability, optical properties and thermal conductivity with saline water-based fluid*. International journal of heat and mass transfer 2017, 107:264-270.
- [51] Kabeel AE, El-Said EMS. *Applicability of flashing desalination technique for small-scale needs using a novel integrated system coupled with the nanofluid-based solar collector*. Desalination 2014, 333(1):10-22.
- [52] Bhadra M, Roy S, Mitra S. *Nanodiamond immobilized membranes for enhanced desalination via membrane distillation*. Desalination 2014, 341:115-119.
- [53] Chen HC, Chen YR, Yang KH, Yang CP, Tung KL, Lee MJ, Shih JH, Liu YC. *Effective reduction of water molecules' interaction for efficient water evaporation in desalination*. Desalination 2018, 436:91-97.
- [54] Agashichev S, Sivakov A. *Modeling and calculation of temperature-concentration polarisation in the membrane distillation process(MD)*. Desalination 1993, 93(1-3):245-258.
- [55] Martinez-Diez L, Vazquez-Gonzalez MI. *Temperature and concentration polarization in membrane distillation of aqueous salt solutions*. J.Membr.Sci. 1999, 156(2):265-273.
- [56] Lin S, Yip NY, Elimelech M. *Direct contact membrane distillation with heat recovery: thermodynamic insights from module scale modeling*. J.Membr.Sci. 2014, 453:498-515.
- [57] Chang H, Liau JS, Ho CD, Wang WH. *Simulation of membrane distillation modules for desalination by developing user's model on Aspen Plus platform*. Desalination 2009, 249(1):380-387.
- [58] Zuo G, Wang R, Field R, Fane AG. *Energy efficiency evaluation and economic analyses of direct contact membrane distillation system using Aspen Plus*. Desalination 2011, 283:237-244.
- [59] Summers EK, Arafat HA, Lienhard V JH. *Energy efficiency comparison of single-stage membrane distillation (MD) desalination cycles in different configurations*. Desalination 2012, 290:54-66.

- [60] S.A.Klein. *Engineering Equation Solver Version 10*.
- [61] Khanafer K, Vafai K. *A critical synthesis of thermophysical characteristics of nanofluids*. International Journal of Heat and Mass Transfer 2011, 54:4410-4428.
- [62] Nkurikiyimfura I, Wang Y, Pan Z. *Heat transfer enhancement by magnetic nanofluids - A review*. Renewable and Sustainable Energy Reviews 2013, 21:548-561.
- [63] Prasher R, Bhattacharya P, Phelan PE. *Thermal Conductivity of Nanoscale Colloidal Solutions (Nanofluids)*. Physical Review Letters 2005, 94(2):025901.
- [64] Li Y, Zhou J, Tung S, Schneider E, Xi S. *A review on development of nanofluid preparation and characterization*. Powder Technology 2009, 196:89-101.
- [65] Das PK. *A review based on the effect and mechanism of thermal conductivity of normal nanofluids and hybrid nanofluids*. Journal of Molecular Liquids 2017, 240:420-446.
- [66] Wang XQ, Mujumdar AS. *Heat transfer characteristics of nanofluids: a review*. International Journal of Thermal Sciences 2007, 46:1-19.
- [67] Koo J, Kleinstreuer C. *A new thermal conductivity model for nanofluids*. Journal of Nanoparticle Research 2004, 6:577-588.
- [68] Yu W, France DM, Routbort JL, Choi S US. *Review and comparison of nanofluid thermal conductivity and heat transfer enhancements*. Heat transfer engineering 2008, 29(5):432-460.
- [69] Mahian O, Kianifar A, Kalogirou SA, Pop I, Wongwises S. *A review of the applications of nanofluids in solar energy*. International Journal of Heat and Mass Transfer 2013, 57(2):582-594.
- [70] Mintsa HA, Roy G, Nguyen CT, Doucet D. *New temperature dependent thermal conductivity data for water-based nanofluids*. International journal of thermal sciences 2009, 48(2):363-371.

- [71] Corcione M. *Empirical correlating equations for predicting the effective thermal conductivity and dynamic viscosity of nanofluids*. Energy conversion and management 2011, 52(1):789-793.
- [72] Nguyen CT, Desgranges F, Roy G, Galanis N, Mare T, Boucher S, Angue Mintsa H. *Temperature and particle-size dependent viscosity data for water-based nanofluids – Hysteresis phenomenon*. International Journal of Heat and Fluid Flow 2007, 28:1492-1506.
- [73] Chapman, S., Cowling, T.G. and Burnett, D. *The mathematical theory of non-uniform gases: an account of the kinetic theory of viscosity, thermal conduction and diffusion in gases*. Cambridge university press, 1990.
- [74] Mahian, O., Kolsi, L., Amani, M., Estellé, P., Ahmadi, G., Kleinstreuer, C., Marshall, J.S., Siavashi, M., Taylor, R.A., Niazmand, H. and Wongwises, S. *Recent advances in modeling and simulation of nanofluid flows-Part I: Fundamentals and theory*. Physics reports 2019, 790:1-48.
- [75] Afrand, M., Najafabadi, K.N. and Akbari, M. *Effects of temperature and solid volume fraction on viscosity of SiO₂-MWCNTs/SAE40 hybrid nanofluid as a coolant and lubricant in heat engines*. Applied Thermal Engineering 2016, 102:45-54.
- [76] Gupta, M., Singh, V., Kumar, R. and Said, Z. *A review on thermophysical properties of nanofluids and heat transfer applications*. Renewable and Sustainable Energy Reviews 2017, 74:638-670.
- [77] Esfe MH, Saedodin S, Mahian O, Wongwises S. *Thermophysical properties, heat transfer and pressure drop of COOH-functionalized multi walled carbon nanotubes/water nanofluids*. Int. Comm. in Heat and Mass Tr. 2014, 58:176-183.
- [78] Peyghambarzadeh SM, Hashemabadi SH, Naraki M, Vermahmoudi Y. *Experimental study of overall heat transfer coefficient in the application of dilute nanofluids in the car radiator*. Applied Thermal Engineering 2013, 52:8-16.

- [79] Sundar LS, Sharma KV, Naik MT, Singh MK. *Empirical and theoretical correlations on viscosity of nanofluids: A review*. Renewable and Sustainable Energy Reviews 2013, 25:670-686.
- [80] Naik MT, Sundar LS. *Investigation into thermophysical properties of glycol based CuO nanofluid for heat transfer applications*. World Academy of Science Eng. Tech. 2011, 59:440-6.
- [81] Assael, M.J., Metaxa, I.N., Arvanitidis, J., Christofilos, D. and Lioutas, C. *Thermal conductivity enhancement in aqueous suspensions of carbon multi-walled and double-walled nanotubes in the presence of two different dispersants*. International Journal of Thermophysics 2005, 26(3), pp.647-664.
- [82] Choi, S.U.S., Zhang, Z.G., Yu, W., Lockwood, F.E. and Grulke, E.A. *Anomalous thermal conductivity enhancement in nanotube suspensions*. Applied physics letters 2001, 79(14), pp.2252-2254.
- [83] Warsinger DM, Nejati S, Fattahijuybari H. *Energy Efficiency Metrics in Membrane Distillation*. Advances in Water Desalination Technologies 2020, b4015-ch08.
- [84] Zhao K, Heinzl W, Wenzel M, Büttner S, Bollen F, Lange G, Heinzl S, Sarda N. *Experimental study of the Memsys vacuum-multi-effect-membrane-distillation (V-MEMD) module*. Desalination 2013, 323:150-160.
- [85] Zaragoza G, Ruiz-Aguirre A, Guillén-Burrieza E. *Efficiency in the use of solar thermal energy of small membrane desalination systems for decentralized water production*. Applied Energy 2014, 130:491-9.
- [86] Andrés-Mañas J.A., Ruiz-Aguirre A., Acién F.G. and Zaragoza G. *Performance increase of membrane distillation pilot scale modules operating in vacuum-enhanced air-gap configuration*. Desalination 2020, 475, p.114202.
- [87] Özerinç, S., Kakaç, S. and Yazıcıoğlu, A.G. *Enhanced thermal conductivity of nanofluids: a state-of-the-art review*. Microfluidics and Nanofluidics 2010, 8(2), pp.145-170.

- [88] Eastman J. A., Choi S. U. S., Li S., Yu W., Thompson L. J. *Anomalously increased effective thermal conductivities of ethylene glycol-based nanofluids containing copper nanoparticles*. Applied physics letters 2001, 78(6), 718-720.
- [89] Chopkar M., Das P. K., Manna I. *Synthesis and characterization of nanofluid for advanced heat transfer applications*. Scripta Materialia 2006, 55(6), 549-552.
- [90] Feng Y., Yu B., Xu P., Zou M. *The effective thermal conductivity of nanofluids based on the nanolayer and the aggregation of nanoparticles*. Journal of Physics D: Applied Physics 2007, 40(10), 3164.
- [91] Prasher R., Phelan P. E., Bhattacharya P. *Effect of aggregation kinetics on the thermal conductivity of nanoscale colloidal solutions (nanofluid)*. Nano letters 2006, 6(7), 1529-1534.
- [92] Rouxel D., Hadji R., Vincent B. and Fort Y. *Effect of ultrasonication and dispersion stability on the cluster size of alumina nanoscale particles in aqueous solutions*. Ultrasonics sonochemistry 2011, 18(1), pp.382-388.
- [93] Mandzy N., Grulke E. and Druffel T. *Breakage of TiO₂ agglomerates in electrostatically stabilized aqueous dispersions*. Powder technology 2005, 160(2), pp.121-126.
- [94] Vasylkiv O., and Sakka Y. *Synthesis and colloidal processing of zirconia nanopowder*. Journal of the American Ceramic Society 2001, 84(11), pp.2489-2494.
- [95] Ma P.C., Siddiqui N.A., Marom G. and Kim J.K. *Dispersion and functionalization of carbon nanotubes for polymer-based nanocomposites: a review*. Composites Part A: Applied Science and Manufacturing 2010, 41(10), pp.1345-1367.
- [96] Boo, C., Lee, J. and Elimelech, M. *Engineering surface energy and nanostructure of microporous films for expanded membrane distillation applications*. Environmental science & technology 2016, 50(15), pp.8112-8119.
- [97] Warsinger DM, Swaminathan J, Burrieza EG, Arifat HA, Lienhard V JH. *Scaling and fouling in membrane distillation for desalination applications: A review*. Desalination 2015, 356:294-313.

- [98] Gayathri N, Sanghyun J, Saravanamuthu V, Tae-Mun H, Yong-Jun C, Seung-Hyun K. *A review on fouling of membrane distillation.* Desalination and Water Treatment 2016, 57(22):10052-10076.